

1 **Temporal variability and driving factors of the carbonate system in the Aransas**  
2 **Ship Channel, TX, USA: A time-series study**

3

4 **Melissa R. McCutcheon<sup>1</sup>, Hongming Yao<sup>1,#</sup>, Cory J. Staryk<sup>1</sup>, Xinping Hu<sup>1</sup>**

5 <sup>1</sup> Harte Research Institute for Gulf of Mexico Studies, Texas A&M University – Corpus  
6 Christi, TX 78412, USA

7 <sup>#</sup> current address: Shenzhen Engineering Laboratory of Ocean Environmental Big Data  
8 Analysis and Application, Shenzhen Institute of Advanced Technology, Chinese  
9 Academy of Sciences, Shenzhen 518055, China

10

11

---

12 *Correspondence to:* Melissa R. McCutcheon ([melissa.mccutcheon@tamucc.edu](mailto:melissa.mccutcheon@tamucc.edu))

13

14

15 **Keywords:** *p*CO<sub>2</sub>, acidification, diel variability, seasonal variability, autonomous sensors

16 **Abstract**

17           The coastal ocean is affected by an array of co-occurring biogeochemical and  
18 anthropogenic processes, resulting in substantial heterogeneity in water chemistry,  
19 including carbonate chemistry parameters such as pH and partial pressure of CO<sub>2</sub> (*p*CO<sub>2</sub>).  
20 To better understand coastal and estuarine acidification and air-sea CO<sub>2</sub> fluxes, it is  
21 important to study baseline variability and driving factors of carbonate chemistry. Using  
22 both discrete bottle sample collection (2014-2020) and hourly sensor measurements  
23 (2016-2017), we explored temporal variability, from diel to interannual scales, in the  
24 carbonate system (specifically pH and *p*CO<sub>2</sub>) at the Aransas Ship Channel located in  
25 northwestern Gulf of Mexico. Using other co-located environmental sensors, we also  
26 explored the driving factors of that variability. Both sampling methods demonstrated  
27 significant seasonal variability at the location, with highest pH (lowest *p*CO<sub>2</sub>) in the  
28 winter and lowest pH (highest *p*CO<sub>2</sub>) in the summer. Significant diel variability was also  
29 evident from sensor data, but the time of day with elevated *p*CO<sub>2</sub>/depressed pH was not  
30 consistent across the entire monitoring period, sometimes reversing from what would be  
31 expected from a biological signal. Though seasonal and diel fluctuations were smaller  
32 than many other areas previously studied, carbonate chemistry parameters were among  
33 the most important environmental parameters to distinguish between time of day and  
34 between seasons. It is evident that temperature, biological activity, freshwater inflow, and  
35 tide level (despite the small tidal range) are all important controls on the system, with  
36 different controls dominating at different time scales. The results suggest that the  
37 controlling factors of the carbonate system may not be exerted equally on both pH and  
38 *p*CO<sub>2</sub> on diel timescales, causing separation of their diel or tidal relationships during

39 certain seasons. Despite known temporal variability on shorter timescales, discrete  
40 sampling was generally representative of the average carbonate system and average air-  
41 sea CO<sub>2</sub> flux on a seasonal and annual basis when compared with sensor data.

## 42 **1. Introduction**

43 Coastal waters, especially estuaries, experience substantial spatial and temporal  
44 heterogeneity in water chemistry—including carbonate chemistry parameters such as pH  
45 and partial pressure of CO<sub>2</sub> (*p*CO<sub>2</sub>)—due to the diversity of co-occurring biogeochemical  
46 and anthropogenic processes (Hofmann et al., 2011; Waldbusser and Salisbury, 2014).  
47 Carbonate chemistry is important because an addition of CO<sub>2</sub> acidifies seawater, and  
48 acidification can negatively affect marine organisms (Barton et al., 2015; Bednaršek et  
49 al., 2012; Ekstrom et al., 2015; Gazeau et al., 2007; Gobler and Talmage, 2014).  
50 Additionally, despite the small surface area of coastal waters relative to the global ocean,  
51 coastal waters are recognized as important contributors in global carbon cycling (Borges,  
52 2005; Cai, 2011; Laruelle et al., 2018).

53 While carbonate chemistry, acidification, and air-sea CO<sub>2</sub> fluxes are relatively  
54 well studied and understood in open ocean environments, large uncertainties remain in  
55 coastal environments. Estuaries are especially challenging to fully understand because of  
56 the heterogeneity between and within estuaries that is driven by diverse processes  
57 operating on different time scales such as river discharge, nutrient and organic matter  
58 loading, stratification, and coastal upwelling (Jiang et al., 2013; Mathis et al., 2012). The  
59 traditional sampling method for carbonate system characterization involving discrete  
60 water sample collection and laboratory analysis is known to lead to biases in average  
61 *p*CO<sub>2</sub> and CO<sub>2</sub> flux calculations due to daytime sampling that neglects to capture diel

62 variability (Li et al., 2018). Mean diel ranges in pH can exceed 0.1 unit in many coastal  
63 environments, and especially high diel ranges (even exceeding 1 pH unit) have been  
64 reported in biologically productive areas or areas with higher mean  $p\text{CO}_2$  (Challener et  
65 al., 2016; Cyronak et al., 2018; Schulz and Riebesell, 2013; Semesi et al., 2009; Yates et  
66 al., 2007). These diel ranges can far surpass the magnitude of the changes in open ocean  
67 surface waters that have occurred since the start of the industrial revolution and rival  
68 spatial variability in productive systems, indicating their importance for a full  
69 understanding of the carbonate system.

70         Despite the need for high-frequency measurements, sensor deployments have  
71 been limited in estuarine environments (especially compared to their extensive use in the  
72 open ocean) because of the challenges associated with varying conditions, biofouling,  
73 and sensor drift (Sastri et al., 2019). Carbonate chemistry monitoring in the Gulf of  
74 Mexico (GOM), has been relatively minimal compared to the United States east and west  
75 coasts. The GOM estuaries currently have less exposure to concerning levels of  
76 acidification than other estuaries because of their high temperatures (causing water to  
77 hold less  $\text{CO}_2$  and support high productivity year-round) and often suitable river  
78 chemistries (i.e., relatively high buffer capacity) (McCutcheon et al., 2019; Yao et al.,  
79 2020). However, respiration-induced acidification is present in both the open GOM (e. g.,  
80 subsurface water influenced by the Mississippi River Plume and outer shelf region near  
81 the Flower Garden Banks National Marine Sanctuary) and GOM estuaries, and most  
82 estuaries in the northwestern GOM have also experienced long-term acidification (Cai et  
83 al., 2011; Hu et al., 2015, 2018; Kealoha et al., 2020; McCutcheon et al., 2019; Robbins  
84 and Lisle, 2018). This known acidification as well as the relatively high  $\text{CO}_2$  efflux from

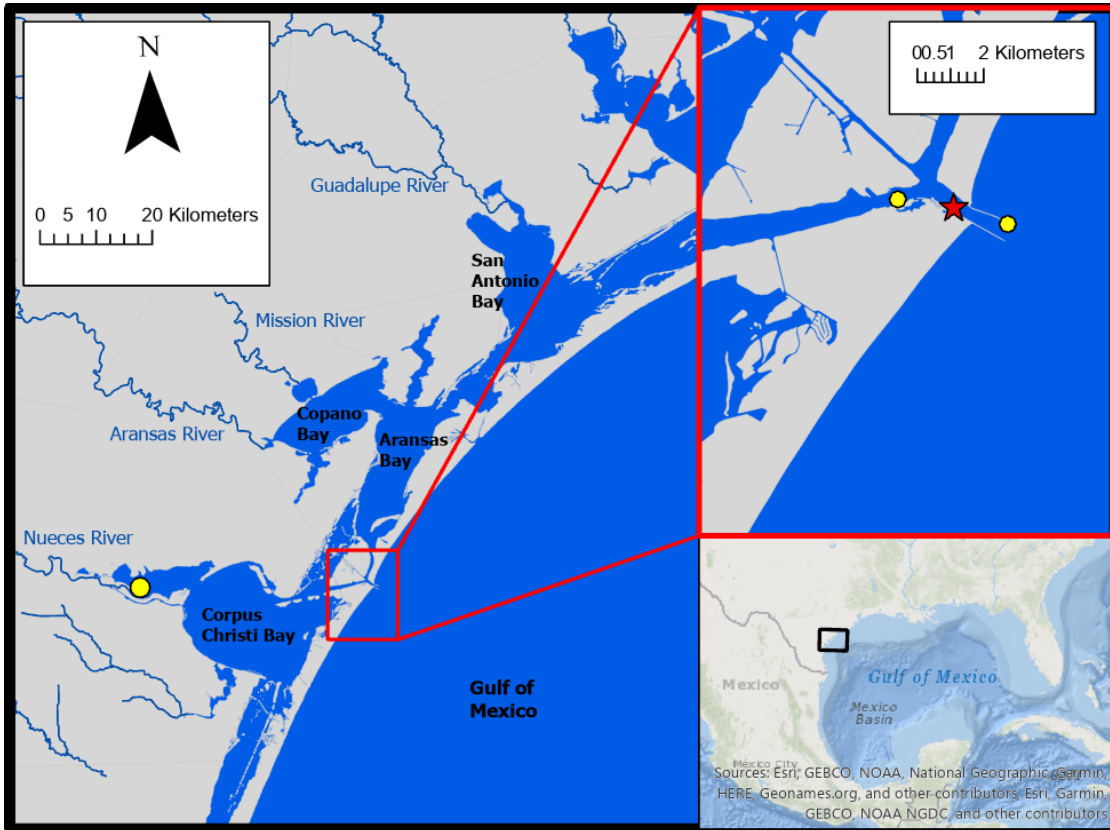
85 the estuaries of the northwest GOM illustrates the necessity to study the baseline  
86 variability and driving factors of carbonate chemistry in the region. In this study, we  
87 explored temporal variability in the carbonate system in Aransas Ship Channel—a tidal  
88 inlet where the lagoonal estuaries meet the coastal waters in a semi-arid region of the  
89 northwestern GOM—using both discrete bottle sample collection and hourly sensor  
90 measurements, and we explored the driving factors of that variability using data from  
91 other co-located environmental sensors.

## 92 **2. Materials and Methods**

### 93 *2.1 Location*

94 Autonomous sensor monitoring and discrete water sample collections for  
95 laboratory analysis of carbonate system parameters were performed in the Aransas Ship  
96 Channel (ASC, located at 27°50'17"N, 97°3'1"W). ASC is one of the few permanent tidal  
97 inlets that intersect a string of barrier islands and connect the GOM coastal waters with  
98 the lagoonal estuaries in the northwest GOM (Fig. 1). ASC provides the direct connection  
99 between the northwestern GOM and the Mission-Aransas Estuary (Copano and Aransas  
100 Bays) to the north and Nueces Estuary (Nueces and Corpus Christi Bays) to the south  
101 (Fig. 1). The region is microtidal, with a small tidal range relative to many other  
102 estuaries, ranging from ~ 0.6 m tides on the open coast to less than 0.3 m in upper  
103 estuaries (Montagna et al., 2011). Mission-Aransas Estuary (MAE) is fed by two small  
104 rivers, the Mission (1787 km<sup>2</sup> drainage basin) and Aransas (640 km<sup>2</sup> drainage basin)  
105 Rivers (<http://waterdata.usgs.gov/>), which both experience low base flows punctuated by  
106 periodic high flows during storm events. MAE has an average residence time of one year  
107 (Solis and Powell, 1999), so there is a substantial lag between time of rainfall and

108 riverine delivery to ASC in the lower estuary. A significant portion of riverine water  
109 flowing into Aransas Bay originates from the larger rivers further northeast on the Texas  
110 coast via the Intracoastal Waterway (i.e., Guadalupe River (26,625 km<sup>2</sup> drainage basin)  
111 feeds San Antonio Bay and has a much shorter residence time of nearly 50 days) (Solis  
112 and Powell, 1999; USGS, 2001).



113  
114 **Figure 1.** Study area. The location of monitoring in the Aransas Ship Channel (red star)  
115 and the locations of NOAA stations used for wind data (yellow circles) are shown.

116  
117 *2.2 Continuous Monitoring*

118 Autonomous sensor monitoring (referred to throughout as continuous monitoring)  
119 of pH and  $p\text{CO}_2$  was conducted from Nov. 8, 2016 to Aug. 23, 2017 at the University of  
120 Texas Marine Science Institute's research pier in ASC. Hourly pH data were collected  
121 using an SATLANTIC® SeaFET pH sensor (on total pH scale) and hourly  $p\text{CO}_2$  data were

122 collected using a Sunburst<sup>®</sup> SAMI-CO<sub>2</sub>. Hourly temperature and salinity data were  
123 measured by a YSI<sup>®</sup> 600OMS V2 sonde. All hourly data were single measurements taken  
124 on the hour. The average difference between sensor pH and discrete quality assurance  
125 samples measured spectrophotometrically in the lab was used to establish a correction (-  
126 0.05) based on a single calibration point across the entire sensor pH dataset (Bresnahan et  
127 al., 2014). See supplemental materials for additional sensor deployment and quality  
128 assurance information.

### 129 *2.3 Discrete Sample Collection and Sample Analysis*

130 Long-term monitoring via discrete water sample collection was conducted at ASC  
131 from May 2, 2014 to February 25, 2020 (in addition to the discrete, quality assurance  
132 sample collections). Sampling was conducted every two weeks during the summer  
133 months and monthly during the winter months from a small vessel at a station near (<20  
134 m from) the sensor deployment. Water sample collection followed standard protocol for  
135 ocean carbonate chemistry studies (Dickson et al., 2007). Ground glass borosilicate  
136 bottles (250 mL) were filled with surface water and preserved with 100  $\mu$ L saturated  
137 mercury chloride (HgCl<sub>2</sub>). Apiezon<sup>®</sup> grease was applied to the bottle stopper, which was  
138 then secured to the bottle using a rubber band and a nylon hose clamp.

139 These samples were used for laboratory dissolved inorganic carbon (DIC) and pH  
140 measurements. DIC was measured by injecting 0.5 mL of sample into 1 ml 10% H<sub>3</sub>PO<sub>4</sub>  
141 (balanced by 0.5 M NaCl) with a high-precision Kloehn syringe pump. The CO<sub>2</sub> gas  
142 produced through sample acidification was then stripped using high-purity nitrogen gas  
143 and carried into a Li-Cor infrared gas detector. DIC analyses had a precision of 0.1%.  
144 Certified Reference Material (CRM) was used to ensure the accuracy of the analysis

145 (Dickson et al. 2003). For samples with salinity > 20, pH was measured using a  
146 spectrophotometric method at  $25 \pm 0.1^\circ\text{C}$  (Carter et al. 2003) and the Douglas and Byrne  
147 (2017) equation. Analytical precision of the spectrophotometric method for pH  
148 measurement was  $\pm 0.0004$  pH units. A calibrated Orion Ross glass pH electrode was  
149 used to measure pH at  $25 \pm 0.1^\circ\text{C}$  for samples with salinity < 20, and analytical precision  
150 was  $\pm 0.01$  pH units. All pH values obtained using the potentiometric method were  
151 converted to total scale at *in situ* temperature (Millero 2001). Salinity of the discrete  
152 samples was measured using a benchtop salinometer calibrated by MilliQ water and a  
153 known salinity CRM. For discrete samples,  $p\text{CO}_2$  was calculated in CO2Sys for Excel  
154 using laboratory-measured salinity, DIC, pH, and *in situ* temperature for calculations.  
155 Carbonate speciation calculations were done using Millero (2010) carbonic acid  
156 dissociation constants ( $K_1$  and  $K_2$ ), Dickson (1990) bisulfate dissociation constant, and  
157 Uppström (1974) borate concentration.

#### 158 2.4 Calculation of $\text{CO}_2$ fluxes

159 Equation 1 was used for air-water  $\text{CO}_2$  flux calculations (Wanninkhof, 1992;  
160 Wanninkhof et al., 2009). Positive flux values indicate  $\text{CO}_2$  emission from the water into  
161 the atmosphere (the estuary acting as a source of  $\text{CO}_2$ ), and negative flux values indicate  
162  $\text{CO}_2$  uptake by the water (the estuary acting as a sink for  $\text{CO}_2$ ).

$$163 F = k K_0 (p\text{CO}_{2,w} - p\text{CO}_{2,a}) \quad (1)$$

164 where  $k$  is the gas transfer velocity (in  $\text{m d}^{-1}$ ),  $K_0$  (in  $\text{mol l}^{-1} \text{atm}^{-1}$ ) is the solubility  
165 constant of  $\text{CO}_2$  (Weiss, 1974), and  $p\text{CO}_{2,w}$  and  $p\text{CO}_{2,a}$  are the partial pressure of  $\text{CO}_2$  (in  
166  $\mu\text{atm}$ ) in the water and air, respectively.



167 We used the wind speed parameterization for gas transfer velocity ( $k$ ) from Jiang  
168 et al. (2008) converted from  $\text{cm h}^{-1}$  to  $\text{m d}^{-1}$ , which is thought to be the best estuarine  
169 parameterization at this time (Crosswell et al., 2017), as it is a composite of  $k$  over  
170 several estuaries. The calculation of  $k$  requires a windspeed at 10 m above the surface, so  
171 windspeeds measured at 3 m above the surface were converted using the power law wind  
172 profile (Hsu, 1994; Yao and Hu, 2017). To assess uncertainty, other parameterizations  
173 with direct applications to estuaries in the literature were also used to calculate  $\text{CO}_2$  flux  
174 (Raymond and Cole 2001; Ho et al. 2006). We note that parameterization of  $k$  based on  
175 solely windspeed is flawed because several additional parameters can contribute to  
176 turbulence including turbidity, bottom-driven turbulence, water-side thermal convection,  
177 tidal currents, and fetch (Wanninkhof 1992, Abril et al., 2009, Ho et al., 2104, Andersson  
178 et al., 2017), however it is currently the best option for this system given the limited  
179 investigations of  $\text{CO}_2$  flux and contributing factors in estuaries.

180 Hourly averaged windspeed data for use in  $\text{CO}_2$  flux calculations were retrieved  
181 from the NOAA-controlled Texas Coastal Ocean Observation Network (TCOON;  
182 <https://tidesandcurrents.noaa.gov/tcoon.html>). Windspeed data from the nearest TCOON  
183 station (Port Aransas Station – located directly in ASC, < 2 km inshore from our  
184 monitoring location) was prioritized when data were available. During periods of missing  
185 windspeed data at the Port Aransas Station, wind speed data from TCOON’s Aransas  
186 Pass Station (< 2 km offshore from monitoring location) were next used, and for all  
187 subsequent gaps, data from TCOON’s Nueces Bay Station (~ 40 km away) were used  
188 (Fig. 1; additional discussion of flux calculation and windspeed data can be found in  
189 supplementary materials). For flux calculations from continuous monitoring data, each

190 hourly measurement of  $p\text{CO}_2$  was paired with the corresponding hourly averaged  
191 windspeed. For flux calculations from discrete sample data, the  $p\text{CO}_2$  calculated for each  
192 sampled day was paired with the corresponding daily averaged windspeed (calculated  
193 from the retrieved hourly averaged windspeeds).

194 Monthly mean atmospheric  $x\text{CO}_2$  data (later converted to  $p\text{CO}_2$ ) for flux  
195 calculations were obtained from NOAA's flask sampling network of the Global  
196 Monitoring Division of the Earth System Research Laboratory at the Key Biscayne (FL,  
197 USA) station. Global averages of atmospheric  $x\text{CO}_2$  were used when Key Biscayne data  
198 were unavailable. Each  $p\text{CO}_2$  observation (whether using continuous or discrete data)  
199 was paired with the corresponding monthly averaged  $x\text{CO}_2$  for flux calculations.  
200 Additional information and justification are available in supplemental materials.

## 201 *2.5 Additional data retrieval and data processing to investigate carbonate system* 202 *variability and controls*

203 All reported annual mean values are seasonally weighted to account for  
204 disproportional sampling between seasons. However, reported annual standard deviation  
205 is associated with the un-weighted, arithmetic mean (Table S1). Temporal variability was  
206 investigated in the form of seasonal and diel variability (Tables S1, S2, S3). For seasonal  
207 analysis, December to February was considered winter, March to May was considered  
208 spring, June to August was considered summer, and September to November was  
209 considered fall. It is important to note that the Fall season had much fewer continuous  
210 sensor observations than other seasons because of the timing of sensor deployment. For  
211 diel comparisons, daytime and nighttime variables were defined as 09:00-15:00 local  
212 standard time and 21:00-03:00 local standard time, respectively, based on the 6-hour

213 periods with highest and lowest photosynthetically active radiation (PAR; data from co-  
 214 located sensor, obtained from the Mission-Aransas National Estuarine Research Reserve  
 215 (MANERR) at <https://missionaransas.org/science/download-data>). Diel ranges in  
 216 parameters were calculated (daily maximum minus daily minimum) and only reported for  
 217 days with the full 24 hours of hourly measurements (176 out of 262 measured days) to  
 218 ensure that data gaps did not influence the diel ranges (Table S3).

219 Controls on  $p\text{CO}_2$  from thermal and non-thermal (i.e., combination of physical  
 220 and biological) processes were investigated following Takahashi et al. (2002) over  
 221 annual, seasonal, and daily time scales using both continuous and discrete data. Over any  
 222 given time period, this method uses the ratio of the ranges of temperature-normalized  
 223  $p\text{CO}_2$  ( $p\text{CO}_{2,nt}$ , Eq. 2) and the mean annual  $p\text{CO}_2$  perturbed by the difference between  
 224 mean and observed temperature ( $p\text{CO}_{2,t}$ , Eq. 3) to calculate the relative influence of non-  
 225 thermal and thermal effects on  $p\text{CO}_2$  (T/B, Eq. 4). When calculating annual T/B values  
 226 with discrete data, only complete years (sampling from January to December) were  
 227 included (2014 and 2020 were omitted). When calculating daily T/B values with  
 228 continuous data, only complete days (24 hourly measurements) were included.

$$229 \quad p\text{CO}_{2,nt} = p\text{CO}_{2,obs} \times \exp[\delta \times (T_{mean} - T_{obs})] \quad (2)$$

$$230 \quad p\text{CO}_{2,t} = p\text{CO}_{2,mean} \times \exp[\delta \times (T_{obs} - T_{mean})] \quad (3)$$

231 where the value for  $\delta$  ( $0.0411 \text{ } ^\circ\text{C}^{-1}$ ), which represents average  $[\partial \ln p\text{CO}_2 / \partial$   
 232 Temperature] from field observations, was taken directly from Yao and Hu (2017),  $T_{obs}$  is  
 233 the observed temperature, and  $T_{mean}$  is the mean temperature over the investigated time  
 234 period.

235 
$$T/B = \frac{\max(pCO_{2,thermal}) - \min(pCO_{2,thermal})}{\max(pCO_{2,non-thermal}) - \min(pCO_{2,non-thermal})} \quad (4)$$

236 Where a T/B greater than one indicates that temperature's control on  $pCO_2$  is greater than  
237 the control from non-thermal factors and a T/B less than one indicates that non-thermal  
238 factors' control on  $pCO_2$  is greater than the control from temperature.

239 Tidal control on parameters was investigated using our continuous monitoring  
240 data and tide level data obtained from NOAA's Aransas Pass Station (the Aransas Pass  
241 Station used for windspeed data, < 2 km offshore from monitoring location, Fig. 1) at  
242 <https://tidesandcurrents.noaa.gov/waterlevels.html?id=8775241&name=Aransas,%20Aransas%20Pass&state=TX>. Hourly measurements of water level were merged with our  
243 sensor data by date and hour. Given that there were gaps in available water level  
244 measurements (and no measurements prior to December 20, 2016), the usable dataset was  
245 reduced from 6088 observations to 5121 observations and fall was omitted from analyses.  
246 To examine differences between parameters during high tide and low tide, we defined  
247 high tide as tide level greater than the third quartile tide level value and low tide as a tide  
248 level less than the first quartile tide level value.

250 Other factors that may exert control on the carbonate system were investigated  
251 through parameter relationships. In addition to previously discussed tide and windspeed  
252 data, we obtained dissolved oxygen (DO), PAR, turbidity, and chlorophyll fluorescence  
253 data from MANERR-deployed environmental sensors that were co-located at our  
254 monitoring location (obtained from <https://missionaransas.org/science/download-data>).  
255 Given that MANERR data are all measured in the bottom water (>5 m) while our sensors  
256 were measuring surface waters, we excluded the observations with significant water  
257 column stratification (defined as a salinity difference > 3 between surface water and

258 bottom water) from analyses. Omitting stratified water reduced our continuous dataset  
259 from 6088 to 5524 observations (removing 260 winter, 133 spring, 51 summer, and 120  
260 fall observations), and omitting observations where there were no MANERR data to  
261 determine stratification further reduced the dataset to 4112 observations. Similarly,  
262 removing instances of stratification reduced discrete sample data from 104 to 89 surface  
263 water observations.

## 264 *2.6 Statistical Analyses*

265 All statistical analyses were performed in R, version 4.0.3 (R Core Team, 2020).  
266 To investigate differences between daytime and nighttime parameter values (temperature,  
267 salinity, pH,  $p\text{CO}_2$ , and  $\text{CO}_2$  flux) using continuous monitoring data across the full  
268 sampling period and within each season, paired  $t$ -tests were used, pairing each respective  
269 day's daytime and nighttime values (Table S3). We also used loess models (locally  
270 weighted polynomial regression) to identify changes in diel patterns over the course of  
271 our monitoring period.

272 Two-way ANOVAs were used to examine differences in parameter means  
273 between seasons and between monitoring methods (Table S2). Since there were  
274 significant interactions (between season and sampling type factors) in the two-way  
275 ANOVAs for each individual parameter (Table S2), differences between seasons were  
276 investigated within each monitoring method (one-way ANOVAs) and the differences  
277 between monitoring methods were investigated within each season (one-way ANOVAs).  
278 For the comparison of monitoring methods, we included both the full discrete sampling  
279 data as well as a subset of the discrete sampling data to overlap with the continuous  
280 monitoring period (referred to throughout as reduced discrete data or  $D_C$ ) along with the

281 continuous data. To interpret differences between monitoring methods, a difference in  
282 means between the continuous monitoring and discrete monitoring datasets would only  
283 indicate that the 10-month period of continuous monitoring was not representative of the  
284 5+ year period that discrete samples have been collected, but a difference in means  
285 between the continuous data and discrete sample data collected during the continuous  
286 monitoring period represents discrepancies between types of monitoring. Post-hoc  
287 multiple comparisons (between seasons within sampling types and between sampling  
288 types within seasons) were conducted using the Westfall adjustment (Westfall, 1997).

289 Differences in parameters between high tide and low tide conditions were  
290 investigated using a two-way ANOVA to model parameters based on tide level and  
291 season. In models for each parameter, there was a significant interaction between tide  
292 level and season factors (based on  $\alpha=0.05$ , results not shown), thus t-tests were used  
293 (within each season) to examine differences in parameters between high and low tide  
294 conditions. Note that fall was omitted from this analysis because tide data were only  
295 available at the location beginning December 20, 2016. Sample sizes were the same for  
296 each parameter (High tide – winter: 354, spring: 569, summer: 350; Low tide – winter:  
297 543, spring: 318, summer: 415).

298 Additionally, to gain insight to carbonate system controls through correlations, we  
299 conducted Pearson correlation analyses to examine individual correlations of pH and  
300  $p\text{CO}_2$  (both continuous and discrete) with other environmental parameters (Table S5).

301 To better understand overall system variability over different time scales, we used  
302 a linear discriminant analysis (LDA), a multivariate statistic that allows dimensional  
303 reduction, to determine the linear combination of environmental parameters (individual

304 parameters reduced into linear discriminants, LDs) that allow the best differentiation  
305 between day and night as well as between seasons. We included  $p\text{CO}_2$ , pH, temperature,  
306 salinity, tide level, wind speed, total PAR, DO, turbidity, and fluorescent chlorophyll in  
307 this analysis. All variables were centered and scaled to allow direct comparison of their  
308 contribution to the system variability. The magnitude (absolute value) of coefficients of  
309 the LDs (Table 1) represents the relative importance of each individual environmental  
310 parameter in the best discrimination between day and night and between seasons, i.e., the  
311 greater the absolute value of the coefficient, the more information the associated  
312 parameter can provide about whether the sample came from day or night (or winter,  
313 spring, or summer). Only one LD could be created for the diel variability (since there are  
314 only two classes to discriminate between – day and night). Two LDs could be created for  
315 the seasonal variability (since there were three classes to discriminate between – fall was  
316 omitted because of the lack of tidal data), but we chose to only report the coefficients for  
317 LD1 given that LD1 captured 95.64% of the seasonal variability.

318

### 319 **3. Results**

#### 320 *3.1 Seasonal variability*

321 Both the continuous and discrete data showed substantial seasonal variability for  
322 all parameters (Fig. 2, Tables S1 and S2). All discrete sample results reported here are for  
323 the entire 5+ years of monitoring; the subset of discrete sample data that overlaps with  
324 the continuous monitoring period will be addressed only in the discussion for method  
325 comparisons (Section 4.1.1). Both continuous and discrete data demonstrate significant  
326 differences in temperature between each season, with the highest temperature in summer

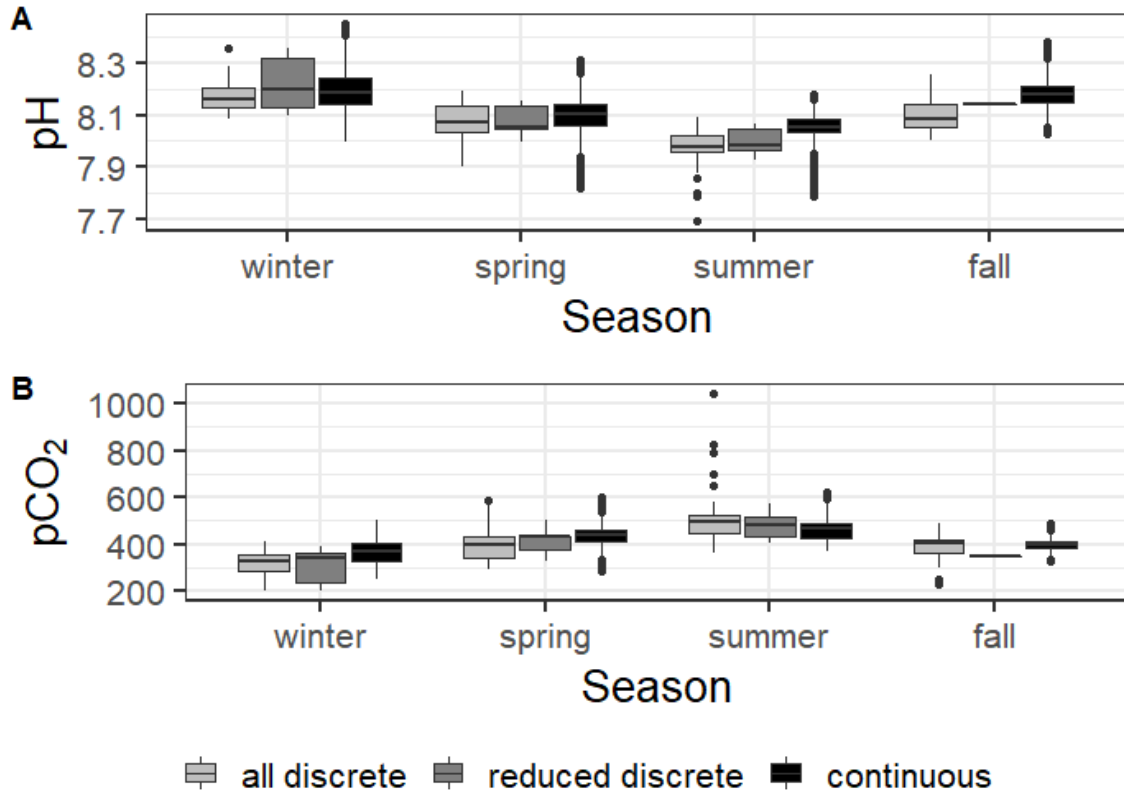
327 and the lowest in winter (Tables S1 and S2). Mean salinity during sampling periods was  
328 highest in the summer and lowest in the fall Table S1). Significant differences in seasonal  
329 salinity occurred between all seasons except spring and winter for continuous data, but  
330 only summer differed from other seasons based on discrete data (Tables S1 and S2).

331         Carbonate system parameters also varied seasonally (Fig. 2). For both continuous  
332 and discrete data, winter had the highest seasonal pH ( $8.19 \pm 0.08$  and  $8.162 \pm 0.065$ ,  
333 respectively) and lowest seasonal  $p\text{CO}_2$  ( $365 \pm 44 \mu\text{atm}$  and  $331 \pm 39 \mu\text{atm}$ ,  
334 respectively), while summer had the lowest seasonal pH ( $8.05 \pm 0.06$  and  $7.975 \pm 0.046$ ,  
335 respectively) and highest seasonal  $p\text{CO}_2$  ( $463 \pm 48 \mu\text{atm}$  and  $511 \pm 108$ , respectively)  
336 (Fig. 2, Table S1). All seasonal differences in pH and  $p\text{CO}_2$  were significant, except for  
337 the discrete data spring versus fall for both parameters (Table S2).

338

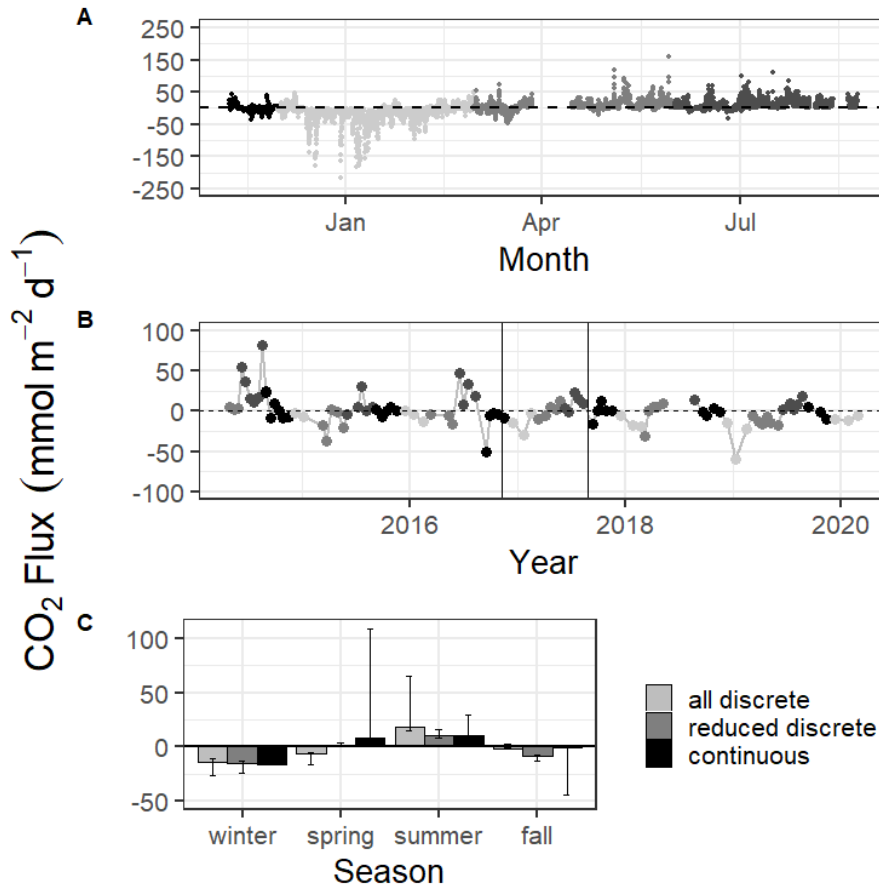
339





340  
 341 **Figure 2.** Boxplots of seasonal variability in pH and  $p\text{CO}_2$  using all discrete data,  
 342 reduced discrete data (to overlap with continuous monitoring, Nov. 8 2016 – Aug 23,  
 343 2017), and continuous sensor data.  
 344

345 Mean  $\text{CO}_2$  flux differed by season (Fig. 3, Tables S1 and S2). Both continuous  
 346 and discrete data records resulted in net negative  $\text{CO}_2$  fluxes during fall and winter  
 347 months, with winter being most negative. Both methods reported a net positive flux for  
 348 summer, while spring fluxes were positive according to continuous data and negative  
 349 according to the 5+ years of discrete data (Fig. 3, Table S1). Annual net  $\text{CO}_2$  fluxes were  
 350 near zero (Table S1).  
 351



352 **Figure 3.** CO<sub>2</sub> flux calculated over the sampling periods from continuous (A) and  
 353 discrete (B) data. Gray scale in (A) and (B) denote different seasons. Vertical lines in (B)  
 354 denote the time period of continuous monitoring. (C) shows the seasonal mean CO<sub>2</sub> flux.  
 355 Error bars represent mean CO<sub>2</sub> flux using Ho (2006) and Raymond and Cole (2001)  
 356 windspeed parameterizations.  
 357  
 358

359 Results of the LDA incorporated carbonate system parameters along with  
 360 additional environmental parameters to get a full picture of system variability over  
 361 seasonal timescales (Table 1). The most important parameter in system variability that  
 362 allowed differentiation between seasons was temperature (Table 1, Seasonal LD1), as  
 363 would be expected with the clear seasonal temperature fluctuations (Fig. S1E). The  
 364 second most important parameter for seasonal differentiation was chlorophyll, likely  
 365 indicating clear seasonal phytoplankton blooms. The carbonate chemistry also played a

366 critical role in seasonal differentiation, as  $p\text{CO}_2$  was the third most important factor  
 367 (Table 1).

368 **Table 1.** Coefficients of linear discriminants (LD) from LDA using continuous sensor  
 369 data and other environmental parameters. Discriminants for both diel and seasonal  
 370 variability shown.

	Seasonal	Diel
	LD1	LD1
Temperature (°C)	-3.53	0.54
Salinity	0.04	0.15
$p\text{CO}_2$ ( $\mu\text{atm}$ )	-0.29	-0.16
pH	0.10	0.06
Tide Level (m)	-0.24	0.10
Wind speed ( $\text{ms}^{-1}$ )	0.05	-0.00
Total PAR	-0.07	-2.29
DO ( $\text{mg L}^{-1}$ )	0.09	-0.08
Turbidity	0.15	-0.06
Fluor. Chlorophyll	-0.40	0.14

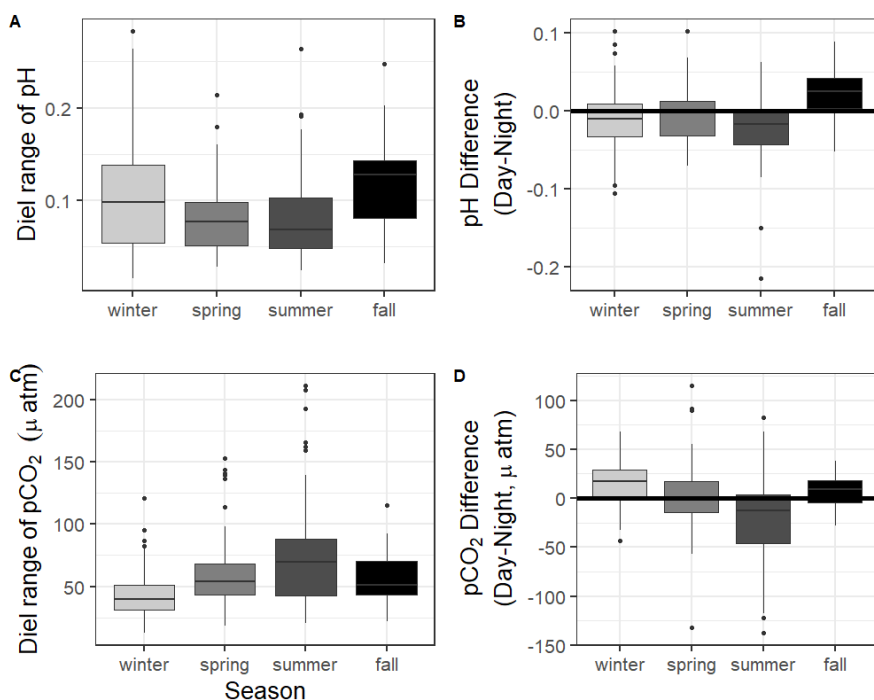
371

### 372 3.2 Diel variability

373 The 10 months of in-situ continuous monitoring revealed that there was  
 374 substantial diel variability in measured parameters (Fig. 4, Table S3). Temperature had a  
 375 mean diel range of  $1.3 \pm 0.8^\circ\text{C}$  (Table S3). Daytime and nighttime temperature differed  
 376 significantly during the summer and fall months, with higher temperatures at night for  
 377 both seasons (Table S3). The mean diel range of salinity was  $3.4 \pm 2.7$  (Table S3).  
 378 Daytime and nighttime salinity differed significantly during the winter and fall months,  
 379 with higher salinities at night for both seasons. The mean diel range of pH was  $0.09 \pm$   
 380  $0.05$  (Table S3). Daytime and nighttime pH differed significantly during the winter,  
 381 summer, and fall, with nighttime pH significantly higher during summer and winter and  
 382 lower during fall (Fig. 4, Table S3). The mean diel range of  $p\text{CO}_2$  was  $58 \pm 33 \mu\text{atm}$  (Fig.  
 383 4, Table S3). Daytime and nighttime  $p\text{CO}_2$  differed significantly during the winter and  
 384 summer months, with nighttime  $p\text{CO}_2$  significantly higher during the summer and lower  
 385 during the winter (Fig. 4, Table S3). No significant difference in daytime and nighttime

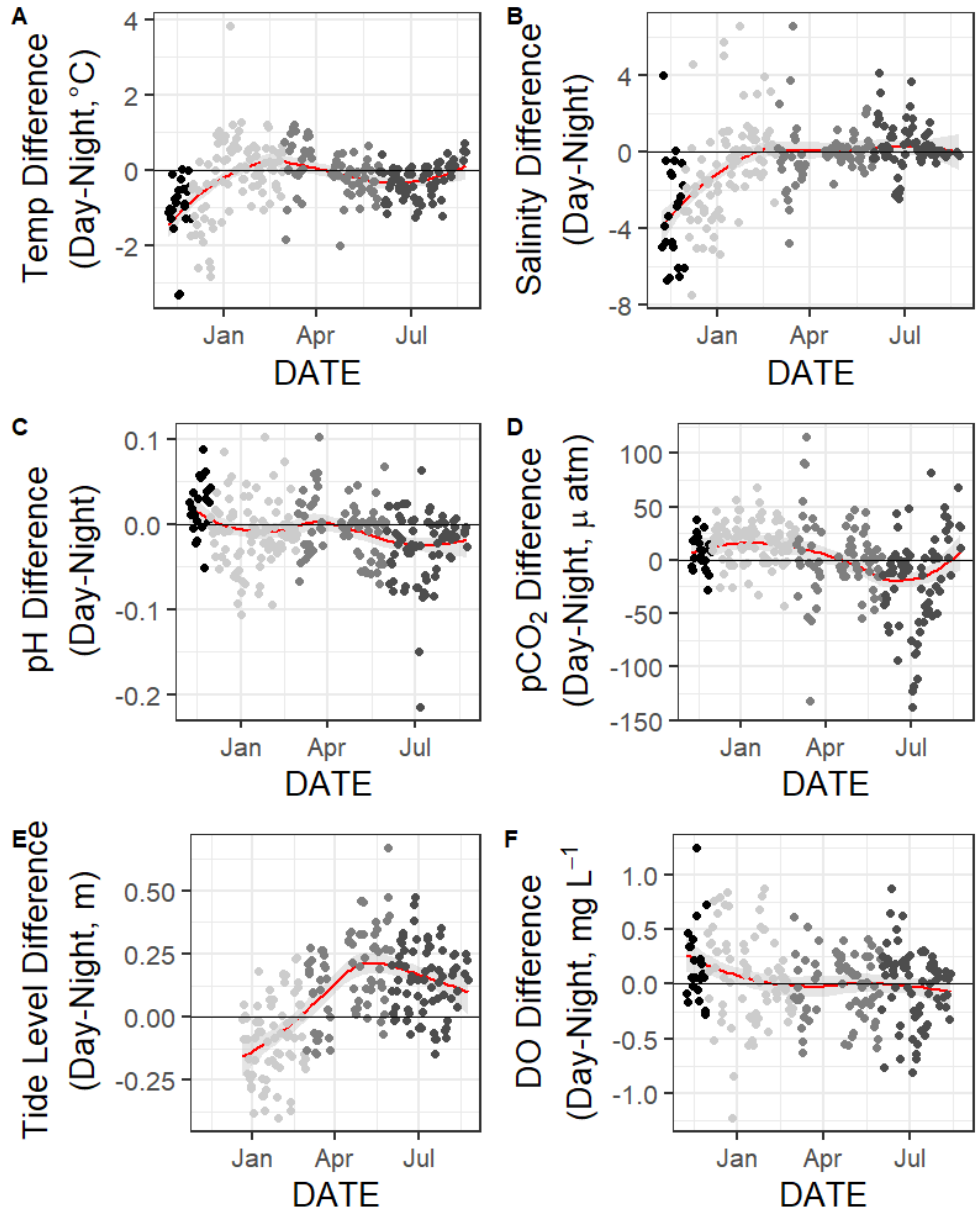
386 DO were observed during any season (Fig. 5F; paired t-tests, winter  $p = 0.1573$ , spring  $p$   
387  $= 0.4877$ , summer  $p = 0.794$ ).

388 Loess models that investigated the evolution of day-night difference in parameters  
389 revealed that other environmental parameters, including salinity, temperature, and tide  
390 level, also had diel patterns that varied over the duration of our continuous monitoring  
391 (Fig. 5).



392 **Figure 4.** Boxplots of the diel range (maximum minus minimum) and difference in daily  
393 parameter mean daytime minus nighttime measurements for pH and  $p\text{CO}_2$  from  
394 continuous sensor data.  
395

396  $\text{CO}_2$  flux also fluctuated on a daily scale, with a mean diel range of  $34.1 \pm 29.0$   
397  $\text{mmol m}^{-2} \text{d}^{-1}$  (Table S3). However, there was not a significant difference in  $\text{CO}_2$  flux of  
398 daytime versus nighttime hours for the entire monitoring period or any individual season  
399 based on  $\alpha=0.05$  (paired t-test, Table S3).  
400



401  
402  
403  
404  
405  
406

**Figure 5.** Loess models (red line) and their confidence intervals (gray bands) showing the difference in daily parameter mean daytime minus nighttime measurements. The gray scale of the data points represents the four seasons over which data were collected

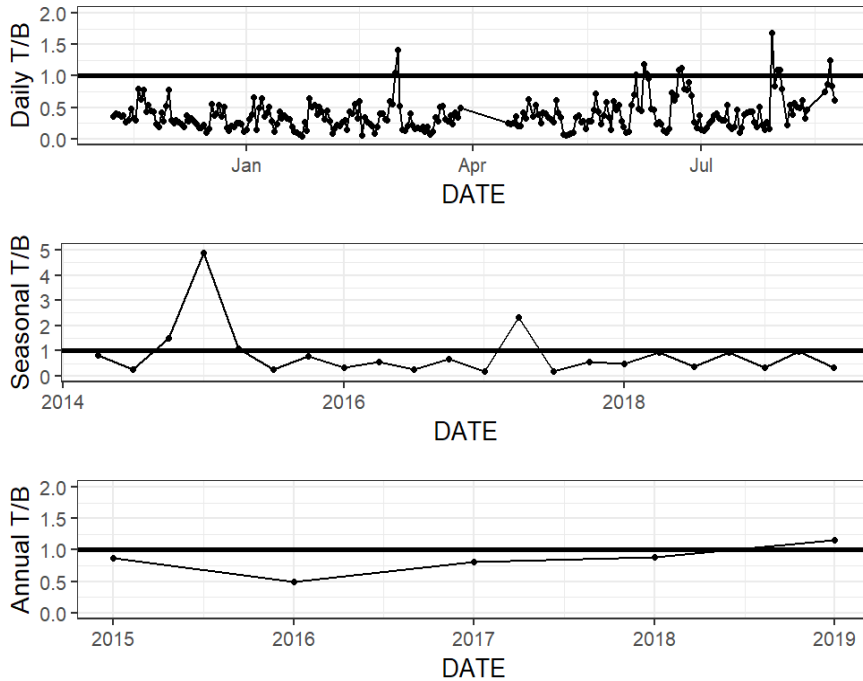
407  
408  
409  
410

Results of the LDA for differentiation between daytime and nighttime conditions revealed that the most important factor was PAR, as would be expected (Table 1, Diel LD1). Temperature was the second most important factor to differentiate between day and night. The carbonate chemistry also played a critical role in day/night differentiation,

411 as  $p\text{CO}_2$  was the third most important parameter, providing more evidence for  
412 differentiation between day and night than other parameters that would be expected to  
413 vary on a diel timescale (e.g., chlorophyll and DO) (Table 1).

### 414 *3.3 Controlling factors and correlates*

415         The relative influence of thermal and non-thermal factors (T/B) in controlling  
416  $p\text{CO}_2$  varied over different time scales (Fig. 6, Table S4). Based on continuous data, non-  
417 thermal processes generally exerted more control than thermal processes ( $T/B < 1$ ) over  
418 the entire 5+ years of discrete monitoring, within each season, and over most (167/178)  
419 days (Fig. 6, Table S4). Annual T/B from discrete data ranged from 0.50 to 1.16, with  
420 only one of the five sampled years having T/B greater than one (i.e., more thermal  
421 influence; Table S4). While most individual seasons that were sampled experienced  
422 stronger non-thermal control on  $p\text{CO}_2$  ( $T/B < 1$ ), the only season that never experienced  
423 stronger thermal control was summer, with summer T/B values ranging from 0.21 – 0.35  
424 for the 6 sampled years (Table S4).



425

426 **Figure 6.** Thermal versus non-thermal control on  $p\text{CO}_2$  daily (top), seasonal (middle),  
 427 and annual (bottom) time scales using both continuous sensor data (daily) and discrete  
 428 sample data (seasonal and annual).  
 429

430 Tidal fluctuations seemed to have a significant effect on carbonate system  
 431 parameters (Table 2). Both temperature and salinity were higher at low tide during the  
 432 winter and summer months and higher at high tide during the spring.  $p\text{CO}_2$  was higher  
 433 during low tide during all seasons. pH was higher during high tide during the winter and  
 434 summer, but this reversed during the spring, when pH was higher at low tide.  $\text{CO}_2$  flux  
 435 also varied with tidal fluctuations.  $\text{CO}_2$  flux was higher (more positive or less negative) in  
 436 the low tide condition for all seasons (though the difference was not significant in  
 437 spring), i.e., the location was less of a  $\text{CO}_2$  sink during low tide conditions in the winter  
 438 and more of a  $\text{CO}_2$  source during low tide conditions in the summer.  
 439

440 **Table 2.** Mean and standard deviation of temperature, salinity, pH,  $p\text{CO}_2$ , and calculated  
 441  $\text{CO}_2$  flux (from continuous sensor measurements) during high and low tide conditions.  
 442

Parameter	Season	High Tide Mean	Low Tide Mean	Difference between tide levels, t-test p-value
<b>Temperature (°C)</b>	Winter	16.7 ± 1.7	17.6 ± 2.0	<0.0001
	Spring	24.4 ± 2.7	23.6 ± 2.7	<0.0001
	Summer	29.3 ± 0.5	30.1 ± 0.7	<0.0001
<b>Salinity</b>	Winter	30.2 ± 2.5	31.3 ± 2.9	<0.0001
	Spring	30.4 ± 1.9	30.0 ± 2.7	0.0071
	Summer	30.5 ± 2.4	34.5 ± 3.0	<0.0001
<b>pH</b>	Winter	8.20 ± 0.08	8.15 ± 0.06	<0.0001
	Spring	8.07 ± 0.09	8.10 ± 0.07	<0.0001
	Summer	8.08 ± 0.04	8.04 ± 0.06	<0.0001
<b><math>p\text{CO}_2</math> (µatm)</b>	Winter	331 ± 40	378 ± 42	<0.0001
	Spring	435 ± 33	443 ± 50	0.0154
	Summer	419 ± 30	482 ± 48	<0.0001
<b><math>\text{CO}_2</math> Flux (mmol m<sup>-2</sup> d<sup>-1</sup>)</b>	Winter	-33.0 ± 38.1	-11.7 ± 21.8	<0.0001
	Spring	7.4 ± 14.0	8.7 ± 14.8	0.2248
	Summer	1.8 ± 6.3	16.0 ± 14.5	<0.0001

443

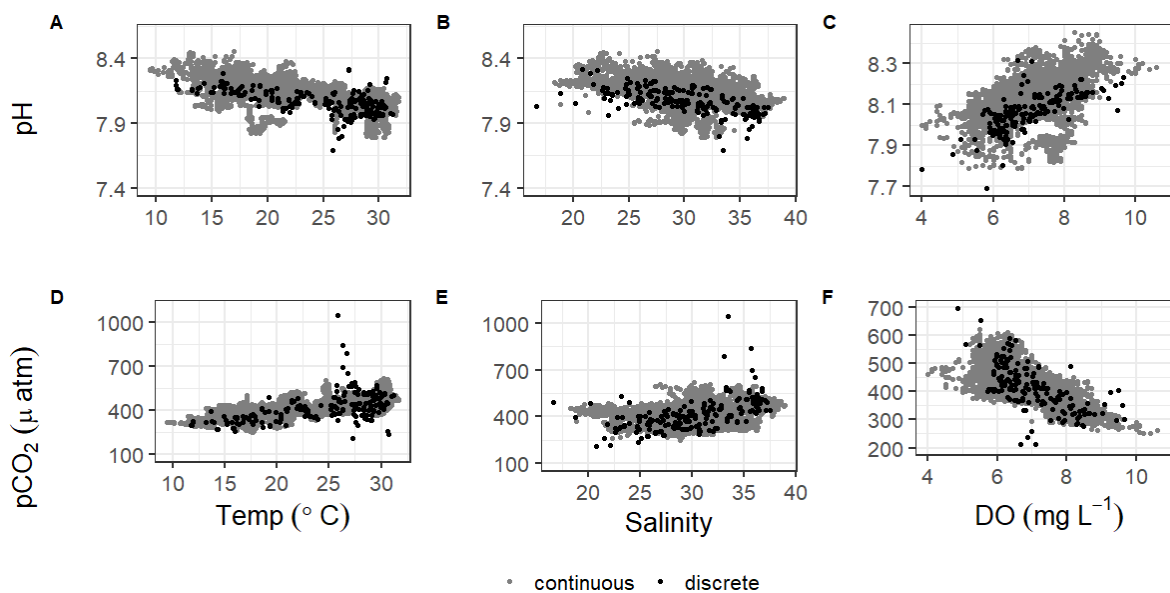
444 Mean water level varied between all seasons; mean spring (highest) water levels  
 445 were on average 0.08 m higher than winter (lowest) water levels (ANOVA  $p < 0.0001$ , fall  
 446 was not considered because of a lack of water level data). The mean daily tidal range  
 447 during our continuous monitoring period was  $0.39 \text{ m} \pm 0.13 \text{ m}$ , which did not  
 448 significantly differ between seasons (ANOVA  $p = 0.739$ ). However, the day-night  
 449 difference in tide level exhibited a strong seasonality, with spring and summer having  
 450 higher tide level during the daytime and winter having higher tide level during the  
 451 nighttime (Fig. 5).

452 There were significant correlations between carbonate system parameters (pH and  
 453  $p\text{CO}_2$ ) and many of the other environmental parameters, including windspeed, DO,  
 454 turbidity, and fluorescent chlorophyll (Figure 7, Table S5). Both the continuous and  
 455 discrete sampling types indicate that pH has a significant negative relationship with both  
 456 temperature and salinity and  $p\text{CO}_2$  has a significant positive relationship with both



457 temperature and salinity (Fig. 7). However, correlations with temperature were stronger  
458 for continuous data and correlations with salinity were stronger for discrete data (Table  
459 S5). The strongest correlations between continuous carbonate system data and all  
460 investigated environmental parameters were with DO (positive correlation with pH and  
461 negative correlation with  $p\text{CO}_2$ ; Table S5). It is worth noting that there were no  
462 observations of hypoxia at our study site during our monitoring, with minimum DO  
463 levels of  $3.9 \text{ mg L}^{-1}$  and  $4.0 \text{ mg L}^{-1}$  for our continuous monitoring period and our discrete  
464 sampling period, respectively.

465  
466



467  
468 **Figure 7.** Correlations of pH and  $p\text{CO}_2$  with temperature, salinity, and DO from  
469 continuous sensor data (gray) and all discrete data (black).  
470

471 **Discussion**

472 *4.1 Comparing continuous monitoring and discrete sampling: Representative sampling in*  
473 *a temporally variable environment*

474 Discrete water sample collection and analysis is the most common method that  
475 has been employed to attempt to understand the carbonate system of estuaries. However,  
476 it is difficult to know if these samples are representative of the spatial and temporal  
477 variability in carbonate system parameters. While this time-series study cannot conclude  
478 whether our broader sampling efforts in the MAE are representative of the spatial  
479 variability in the estuary, it can investigate how representative our bimonthly to monthly  
480 sampling is of the more high-frequency temporal variability that ASC experiences.

481 There were several instances where seasonal parameter means significantly  
482 differed between the 10-month continuous monitoring period and the 5+ year discrete  
483 sampling period (Table S2,  $C \neq D$  or  $D_c \neq D$ ) including temperature in the summer and  
484 fall, salinity in the spring, pH in the summer and fall, and  $p\text{CO}_2$  in winter, spring, and  
485 summer. While clear seasonal variability was demonstrated for most parameters (using  
486 both continuous and discrete data for the entire period), these differences between the 10-  
487 month continuous monitoring period and our 5+ year monitoring period illustrate that  
488 there is also interannual variability in the system. Therefore, short periods of monitoring  
489 are unable to fully capture current baseline conditions.

490 During the continuous monitoring period (2016-2017), we found no significant  
491 difference between sampling methods in the seasonal mean temperature, salinity, or  
492  $p\text{CO}_2$ . The two sampling methods also resulted in the same mean pH for all seasons  
493 except for summer, when the sensor data recorded a higher mean pH than discrete

494 samples (Tables S1 and S2). During this case, we can conclude that discrete monitoring  
495 did not accurately represent the system variability that was able to be captured by the  
496 sensor monitoring. However, given that most seasons did not show differences in pH or  
497  $p\text{CO}_2$  between sampling methods, the descriptive statistics associated with the discrete  
498 monitoring did a fair job of representing system means. This is evidence that long-term  
499 discrete monitoring efforts, which are much more widespread in estuarine systems than  
500 sensor deployments, can be generally representative of the system despite known  
501 temporal variability on shorter time scales. However, further study would be needed to  
502 determine if this applies throughout the system, as the upper estuary generally  
503 experiences greater variability.

504         Understanding the relationships of pH and  $p\text{CO}_2$  with temperature and salinity is  
505 important in a system (Fig. 7). Based on the results of an Analysis of Covariance  
506 (ANCOVA), the relationship (slope) of pH with both temperature and salinity and of  
507  $p\text{CO}_2$  with salinity were not significantly different between types of monitoring  
508 (considering the sensor deployment period only), supporting the effectiveness of long-  
509 term discrete monitoring programs when sensors are unable to be deployed. However,  
510 ANCOVA did reveal the relationship of  $p\text{CO}_2$  with temperature is significantly different  
511 (method:temp  $p=0.0062$ ) between monitoring methods.

512         The high temporal resolution of sensor data is presumably better for estimating  
513  $\text{CO}_2$  flux at a given location than discrete sampling. Previous studies have pointed out  
514 that discrete sampling methods, which generally involve only daytime sampling, do not  
515 adequately capture the diel variability in the carbonate system and may therefore lead to  
516 underestimation of  $\text{CO}_2$  fluxes. However, we found no significant difference (within any

517 season) between CO<sub>2</sub> flux values calculated with sensor data versus discrete samples  
518 (Table S2, Fig. 3). Calculated CO<sub>2</sub> fluxes also did not significantly differ between day  
519 and night during any season, despite some differences in *p*CO<sub>2</sub> (Table S3), likely due to  
520 the large error associated with the calculation of CO<sub>2</sub> flux (Table S1, Fig. 3) which will  
521 be further discussed below. Therefore, the expected underestimation of CO<sub>2</sub> flux based  
522 on diel variability of *p*CO<sub>2</sub> was not encountered at our study site, validating the use of  
523 discrete samples for quantification of CO<sub>2</sub> fluxes (until methods with less associated error  
524 are available). Even given less error in calculated flux, estimated fluxes would likely not  
525 differ between methods on an annual scale (as *p*CO<sub>2</sub> did not), but CO<sub>2</sub> fluxes may differ  
526 on a seasonal scale since the differences between daytime and nighttime *p*CO<sub>2</sub> were not  
527 consistent across seasons (Table S3, Fig. 4).

528         There are many factors contributing to error associated with CO<sub>2</sub> flux. There is  
529 still large error associated with estimates of estuarine CO<sub>2</sub> flux because turbulent mixing  
530 is difficult to model and turbulence is the main control on CO<sub>2</sub> gas transfer velocity, *k*, in  
531 shallow water environments. Thus, our wind speed parameterization of *k* is imperfect and  
532 likely the greatest source of error. Other notable sources of error include the data  
533 treatment. For example, we chose to seasonally weight the individual calculated flux  
534 values in the calculation of annual flux to account for differences in sampling frequency  
535 between seasons. From continuous data, the weighted average flux was 0.2 mmol m<sup>-2</sup> d<sup>-1</sup>,  
536 although choosing not to seasonally weight and simply look at the arithmetic mean of  
537 fluxes calculated directly from sampling dates would have resulted in an annual CO<sub>2</sub> flux  
538 of -0.7 mmol m<sup>-2</sup> d<sup>-1</sup> for the same period. Similarly, the weighted average flux from all 5+  
539 years of discrete data was -0.9 mmol m<sup>-2</sup> d<sup>-1</sup>, but the arithmetic mean of fluxes would

540 have resulted in an annual CO<sub>2</sub> flux of 0.2 mmol m<sup>-2</sup> d<sup>-1</sup> for the same period. Another  
541 source of error that could be associated with the calculation of flux from the discrete data  
542 is the way in which wind speed data are aggregated to be used in the windspeed  
543 parameterization. We decided to use daily averages of the windspeed for calculations.  
544 Using the windspeed measured for the closest time to our sampling time or the monthly  
545 averaged wind speed may have resulted in very different flux values.

546

#### 547 *4.2 Factors controlling temporal variability in carbonate system parameters*

548 Our study site had a relatively small range of pH and pCO<sub>2</sub> on both diel and  
549 seasonal scales compared to other coastal regions (Challener et al., 2016; Yates et al.,  
550 2007). This small variability is likely tied to a combination of the subtropical setting  
551 (small temperature variability), the lower estuary position of our monitoring (further  
552 removed from the already small freshwater influence), little ocean upwelling influence,  
553 and the system's relatively high buffer capacity that results from the high alkalinity of the  
554 freshwater endmembers (Yao et al., 2020). Just as the extent of hypoxia-induced  
555 acidification was relatively low in Corpus Christi Bay because of the bay's high buffer  
556 capacity (McCutcheon et al., 2019), the extent of pH fluctuation resulting from all  
557 controlling factors at ASC would also be modulated by the region's high intrinsic buffer  
558 capacity.

559 We demonstrated that both temperature and non-thermal processes exert control  
560 on pCO<sub>2</sub>, but non-thermal control generally surpasses thermal control in ASC over  
561 multiple time scales (Fig. 6, Table S4, T/B<1). The magnitude of pCO<sub>2</sub> variation  
562 attributed to non-thermal processes varied greatly (i.e., ΔpCO<sub>2,nt</sub> had large standard  
563 deviations, Table S4). For example, during the year of strongest non-thermal control

564 (2016),  $\Delta p\text{CO}_{2,\text{nt}}$  was 534  $\mu\text{atm}$  versus  $\Delta p\text{CO}_{2,\text{nt}}$  of 209  $\mu\text{atm}$  in the year of weakest  
565 thermal control (2019). Conversely, the magnitude of  $p\text{CO}_2$  variation attributed to  
566 temperature was consistent across time scales. For example, during the year of strongest  
567 thermal control (2015),  $\Delta p\text{CO}_{2,\text{t}}$  was 276  $\mu\text{atm}$  versus  $\Delta p\text{CO}_{2,\text{t}}$  of 242  $\mu\text{atm}$  in the year of  
568 weakest thermal control (2017). Spring and fall seasons, which experienced the greatest  
569 temperature swings (Table S1), had greater relative temperature control exerted on  $p\text{CO}_2$   
570 out of all seasons (Fig. 6, Table S4). The difference in T/B between sampling methods is  
571 relatively small over the 10-month sensor deployment period, but it is worth noting that  
572 T/B did not align over shorter seasonal time scales sampling methods (Fig. 6, Table S4).  
573 Continuous monitoring demonstrated a greater magnitude of fluctuation resulting from  
574 both temperature and non-thermal processes (i.e., greater  $\Delta p\text{CO}_{2,\text{t}}$  and  $\Delta p\text{CO}_{2,\text{nt}}$ ),  
575 indicating that the extremes are generally not captured by the discrete, daytime sampling,  
576 and sensor data would provide a better understanding of system controls.

577         The greater influence of non-thermal controls that we report conflicts with Yao  
578 and Hu (2017), who found that ASC was primarily thermally controlled (T/B 1.53 – 1.79)  
579 from May 2014 to April 2015. Yao and Hu (2017) also found that locations in the upper  
580 estuary experienced lower T/B during flooding conditions than drought conditions.  
581 Although the opposite was found at ASC, it is likely that the high T/B calculated at ASC  
582 by Yao and Hu (2017) was still a result of the drought condition due to the long residence  
583 time of the estuary. Since 2015, there has not been another significant drought in the  
584 system, so it seems that non-thermal controls on  $p\text{CO}_2$  are more important at this location  
585 under normal freshwater inflow conditions.

586           Significantly warmer water temperatures were observed during the nighttime in  
587 both summer and fall (Fig. 5), indicating that temperature could exert a slight control on  
588 the carbonate system over a diel time scale. We note that significant differences in day  
589 and night temperature within seasons do not indicate that diel differences were observed  
590 on all days within the season, as large standard deviations in both daytime and nighttime  
591 values result in considerable overlap. More substantial temperature swings between  
592 seasons would result in more temperature control over a seasonal timescale. ASC seems  
593 to have less thermal control of the carbonate system than offshore GOM waters, as  
594 temperature had substantially higher explanatory value for pH and  $p\text{CO}_2$  based on simple  
595 linear regressions in offshore GOM waters ( $R^2 = 0.81$  and  $0.78$ , respectively (Hu et al.,  
596 2018)) than at ASC ( $R^2 = 0.30$  and  $0.52$ , respectively, for sensor data and  $R^2 = 0.38$  and  
597  $0.25$ , respectively, for discrete data).

598           Though annual average  $p\text{CO}_2$  (and  $\text{CO}_2$  flux) are higher in the upper MAE and  
599 lower offshore than at our study site, the same seasonal patterns that we observed (i.e.,  
600 elevated  $p\text{CO}_2$  and positive  $\text{CO}_2$  flux in the summer and depressed  $p\text{CO}_2$  and negative  
601  $\text{CO}_2$  flux during the winter, Table S1, Fig. S1) has also been observed throughout the  
602 entire MAE and the open Gulf of Mexico (Hu et al., 2018; Yao and Hu, 2017). These  
603 seasonal patterns correspond with both the directional response of the system to  
604 temperature and net community metabolism response to changing temperature, i.e.,  
605 elevated respiration in summer months (Caffrey, 2004). Despite that there were no  
606 observations of hypoxia, there was a strong relationship between the carbonate system  
607 parameters and DO (Fig. 7, Table S5), suggesting that net ecosystem metabolism may  
608 exert an important control on the carbonate system on certain time scales. The lack of

609 day-night difference in DO (Fig. 5F) despite the significant day-night difference in both  
610 pH and  $p\text{CO}_2$  suggests that net community metabolism is likely not a strong controlling  
611 factor on diel time scales. Biological control likely becomes more important over  
612 seasonal timescales.

613         While the tidal range in the northwestern GOM is relatively small (1.30 m over  
614 our 10-month continuous monitoring period), the tidal inlet location of our study site  
615 results in proportionally more “coastal water” during high tide and proportionally more  
616 “estuarine water” during low tide. The carbonate chemistry signal of these different water  
617 masses was seen in the differences between high tide and low tide conditions at ASC  
618 (i.e., high tide having lower  $p\text{CO}_2$  because coastal waters are less heterotrophic than  
619 estuarine waters, Table 2). Consequently, the relative importance of thermal versus non-  
620 thermal controls may be modulated by tide level. We calculated the thermal and non-  
621 thermal  $p\text{CO}_2$  terms separately during high tide and low tide periods and found that non-  
622 thermal control is more important during low tide conditions (within each season T/B is  
623  $0.10 \pm 0.07$  lower during the low tide than high tide). This is likely because low tide has  
624 proportionally more “estuarine water” at the location and because there is less volume of  
625 water for the end products of biological processes to accumulate. The difference in T/B  
626 between high tide and low tide conditions was greatest in the spring, likely due to a  
627 combination of elevated spring-time productivity and larger tidal ranges in the spring.

628         The GOM is one of the few places in the world that experiences diurnal tides  
629 (Seim et al., 1987; Thurman, 1994), so theoretically, the fluctuations in  $p\text{CO}_2$  associated  
630 with tides may align to either amplify or reduce/reverse the fluctuations that would result  
631 from diel variability in net community metabolism. Based on diel tidal fluctuations at this



632 site (i.e., higher tides during the day in the spring and summer and higher tides at night  
633 during the winter, Fig. 5E) and the higher  $p\text{CO}_2$  associated with low tide (Table 2), tidal  
634 control should amplify the biological signal (nighttime  $p\text{CO}_2 > \text{daytime } p\text{CO}_2$ ) during  
635 spring and summer and reduce or reverse the biological signal during the winter. This  
636 tidal control can explain the diel variability present in our  $p\text{CO}_2$  data, which showed the  
637 full reversal of the expected biological signal in the winter (Fig. 5C, Table S3, nighttime  
638  $p\text{CO}_2 < \text{daytime } p\text{CO}_2$ ), i.e., the higher nighttime tides in winter brought in enough low  
639  $\text{CO}_2$  water from offshore to fully offset any nighttime buildup of  $\text{CO}_2$  from the lack of  
640 photosynthesis. However, we note that the expected diel, biological control was likely  
641 minimal since daytime DO was not consistently higher than nighttime DO (Fig. 5F). The  
642 same seasonal pattern diel tide fluctuations were exhibited from Dec 20, 2016 (when the  
643 tide data is first available) through the rest of our discrete monitoring period (Feb 25,  
644 2020), indicating that tidal control on diel variability of carbonate system parameters was  
645 likely consistent throughout this 3+ year period. The diel variability in pH did not mirror  
646  $p\text{CO}_2$  as would be expected (Fig. 5). The relationship between pH and tide level more  
647 closely mirrored the relationships of salinity and temperature with tide level (versus  $p\text{CO}_2$   
648 relationship with tide level; Table 2), indicating that controlling factors of the carbonate  
649 system may not be exerted equally on both pH and  $p\text{CO}_2$  over different time scales.

650 Previous studies have indicated that freshwater inflow may exert a primary  
651 control on the carbonate system in the estuaries of the northwestern GOM (Hu et al.,  
652 2015; Yao et al., 2020; Yao and Hu, 2017). Carbonate system variability is much lower at  
653 ASC than it is in the more upper reaches of MAE, likely due to the lesser influence of  
654 freshwater inflow and its associated changes in biological activity at ASC (Yao and Hu,

655 2017). Given the location of our sampling in the lower portion of the estuary and the  
656 long residence time in the system, we did not directly address river discharge as a  
657 controlling factor, but the influence of freshwater inflow may be evident in the response  
658 of the system to changes in salinity. Fluctuating salinity at ASC may also result from  
659 direct precipitation, stratification, and tidal fluctuations; however, the low  $R^2$  (0.02)  
660 associated with a simple linear regression between tide level and salinity ( $p < 0.0001$ )  
661 indicates that salinity fluctuations are more indicative of non-tidal factors. Salinity data  
662 from both sensor and discrete monitoring were strongly correlated with both pH and  
663  $p\text{CO}_2$ , with correlation coefficients nearing (continuous) or surpassing (discrete) that of  
664 the correlations with temperature (Fig. 7; Table S5). Periods of lower salinity had higher  
665 pH and lower  $p\text{CO}_2$ , likely due to enhanced freshwater influence and subsequent elevated  
666 primary productivity at the study site.

667 We investigated wind speed as a possible control on the carbonate system to gain  
668 insight into the effect of wind-driven  $\text{CO}_2$  fluxes on the inventory of  $\text{CO}_2$  in the water  
669 column (and subsequent impacts to the entire carbonate system). The Texas coast has  
670 relatively high wind speeds, with the mean wind speed observed during our continuous  
671 monitoring period being  $5.8 \text{ m s}^{-1}$ . While this results in relatively high calculated  $\text{CO}_2$   
672 fluxes (Fig. 3), the seasonal relationship between  $p\text{CO}_2$  and windspeed does not support a  
673 change in inventory with higher winds. Since spring and summer both have a mean  
674 estuarine  $p\text{CO}_2$  greater than atmospheric level (and positive  $\text{CO}_2$  flux, Table S1) a  
675 negative relationship between windspeed and  $p\text{CO}_2$  would be necessary to support this  
676 hypothesis, but winter, spring, and fall all experience increases in  $p\text{CO}_2$  with increasing  
677 wind based on simple linear regression.

#### 678 *4.3 Carbonate chemistry as a component of overall system variability*

679           Estuaries and coastal areas are dynamic systems with human influence, riverine  
680 influence, and influence from an array of biogeochemical processes, resulting in highly  
681 variable environmental conditions. Based on an LDA used to assess overall system  
682 variability using a suite of environmental parameters compiled at a single location, we  
683 can conclude that carbonate chemistry parameters are among the most important of  
684 variants on both daily and seasonal time scales in this coastal setting. Of the two  
685 carbonate system components that we incorporated (pH and  $p\text{CO}_2$ ),  $p\text{CO}_2$  was the most  
686 critical in discriminating along diel or seasonal scales despite similar seasonal differences  
687 that were identified by ANOVA (Table S2) and more seasons with significant diel  
688 differences in pH (Table S3). pH seemed to be a larger component of overall system  
689 variability on a seasonal time scale (compared to the very small contribution seen on a  
690 diel scale, Table 1). Given that the seasonal and diel variability in carbonate chemistry at  
691 this location is relatively small compared to other coastal areas that are in the literature,  
692 the high contribution of carbonate chemistry to overall system variability that we detected  
693 is likely to be present at other coastal locations around the world.

#### 694 **5. Conclusions**

695           We monitored carbonate chemistry parameters (pH and  $p\text{CO}_2$ ) using both sensor  
696 deployments (10 months) and discrete sample collection (5+ years) at the Aransas Ship  
697 Channel, TX, to characterize temporal variability. Significant seasonal variability and  
698 diel variability in carbonate system parameters were both present at the location. Diel  
699 fluctuations were smaller than many other areas previously studied. The difference  
700 between daytime and nighttime values of carbonate system parameters varied between

701 seasons, occasionally reversing the expected diel variability due to biological processes.  
702 Tide level (despite the small tidal range), temperature, freshwater influence, and  
703 biological activity all seem to exert important controls on the carbonate system at the  
704 location. The relative importance of the different controls varied with timescale, and  
705 controls were not always exerted equally on both pH and  $p\text{CO}_2$ . Carbonate chemistry  
706 (particularly  $p\text{CO}_2$ ) was among the most important environmental parameters to in  
707 overall system variability to distinguish between both diel and seasonal environmental  
708 conditions.

709         Despite known temporal variability on shorter timescales, discrete sampling was  
710 generally representative of the average carbonate system on a seasonal and annual basis  
711 based on comparison with our sensor data. Additionally, there was no difference in  $\text{CO}_2$   
712 flux between sampling types, supporting the validity of discrete sample collection for  
713 carbonate system characterization at this location.

714         This is one of the first studies that investigates high-temporal frequency data from  
715 deployed sensors that measure carbonate system parameters in an estuary-influenced  
716 environment. Long-term, effective deployments of these monitoring tools could greatly  
717 improve our understanding of estuarine systems. This study's detailed investigation of  
718 data from multiple, co-located environmental sensors was able to provide insight into  
719 potential driving forces of carbonate chemistry on diel and seasonal time scales; this  
720 provides strong support for the implementation of carbonate chemistry monitoring in  
721 conjunction with preexisting coastal environmental monitoring infrastructure.

722         Strategically locating such sensors in areas that are subject to local acidification drivers  
723 or support large biodiversity or commercially important species may be the most crucial

724 in guiding future mitigation and adaptation strategies for natural systems and aquaculture  
725 facilities.

726

#### 727 **Data availability**

728 Continuous sensor data are archived with the National Oceanic and Atmospheric  
729 Administration's (NOAA's) National Centers for Environmental Information (NCEI)  
730 (<https://doi.org/10.25921/dkg3-1989>). Discrete sample data are available in two separate  
731 datasets archived with National Science Foundation's Biological & Chemical  
732 Oceanography Data Management Office (BCO-DMO) (doi:10.1575/1912/bco-  
733 dmo.784673.1 and doi: 10.26008/1912/bco-dmo.835227.1).

#### 734 **Author Contribution**

735 MM and XH defined the scope of this work. XH received funding for all components of  
736 the work. MM, HY, and CJS performed field sampling and laboratory analysis of  
737 samples. MM prepared the initial manuscript and all co-authors contributed to revisions.

#### 738 **Competing interests**

739 The authors declare that they have no conflict of interest.

740

#### 741 **Acknowledgements**

742 Funding for autonomous sensors and sensor deployment was provided by the  
743 United States Environmental Protection Agency's National Estuary Program via the  
744 Coastal Bend Bays and Estuaries Program Contract No. 1605. Thanks to Rae Mooney  
745 from Coastal Bend Bays and Estuaries Program for assistance in the initial sensor setup.

746 Funding for discrete sampling as well MM's dissertation research has been supported by  
747 both NOAA National Center for Coastal Ocean Science (Contract No.  
748 NA15NOS4780185) and NSF Chemical Oceanography Program (OCE-1654232). We  
749 also appreciate the support from the Mission-Aransas National Estuarine Research  
750 Reserve in allowing us the boat-of-opportunity for our ongoing discrete sample  
751 collections and the University of Texas Marine Science Institute for allowing us access to  
752 their research pier for the sensor deployment. A special thanks to Hongjie Wang, Lisette  
753 Alcocer, Allen Dees, and Karen Alvarado for assistance with field work.

#### 754 **References**

- 755 Barton, A., Waldbusser, G.G., Feely, R.A., Weisberg, S.B., Newton, J.A., Hales, B.,  
756 Cudd, S., Eudeline, B., Langdon, C.J., Jefferds, I., King, T., Suhrbier, A.,  
757 Mclaughlin, K., 2015. Impacts of coastal acidification on the pacific northwest  
758 shellfish industry and adaptation strategies implemented in response. *Oceanography*  
759 28, 146–159.
- 760 Bednaršek, N., Tarling, G.A., Bakker, D.C.E., Fielding, S., Jones, E.M., Venables, H.J.,  
761 Ward, P., Kuzirian, A., Lézé, B., Feely, R.A., Murphy, E.J., 2012. Extensive  
762 dissolution of live pteropods in the Southern Ocean. *Nat. Geosci.* 5, 881–885.  
763 <https://doi.org/10.1038/ngeo1635>
- 764 Borges, A. V., 2005. Do we have enough pieces of the jigsaw to integrate CO<sub>2</sub> fluxes in  
765 the coastal ocean? *Estuaries* 28, 3–27.
- 766 Bresnahan, P.J., Martz, T.R., Takeshita, Y., Johnson, K.S., LaShomb, M., 2014. Best  
767 practices for autonomous measurement of seawater pH with the Honeywell Durafet.  
768 *Methods Oceanogr.* 9, 44–60. <https://doi.org/10.1016/j.mio.2014.08.003>

769 Caffrey, J.M., 2004. Factors controlling net ecosystem metabolism in U.S. estuaries.  
770 *Estuaries* 27, 90–101. <https://doi.org/10.1007/BF02803563>

771 Cai, W.-J., 2011. Estuarine and coastal ocean carbon paradox: CO<sub>2</sub> sinks or sites of  
772 terrestrial carbon incineration? *Ann. Rev. Mar. Sci.* 3, 123–145.  
773 <https://doi.org/10.1146/annurev-marine-120709-142723>

774 Cai, W.-J., Hu, X., Huang, W.-J., Murrell, M.C., Lehrter, J.C., Lohrenz, S.E., Chou, W.-  
775 C., Zhai, W., Hollibaugh, J.T., Wang, Y., Zhao, P., Guo, X., Gundersen, K., Dai, M.,  
776 Gong, G.-C., 2011. Acidification of subsurface coastal waters enhanced by  
777 eutrophication. *Nat. Geosci.* 4, 766–770. <https://doi.org/10.1038/ngeo1297>

778 Challener, R.C., Robbins, L.L., McClintock, J.B., 2016. Variability of the carbonate  
779 chemistry in a shallow, seagrass-dominated ecosystem: Implications for ocean  
780 acidification experiments. *Mar. Freshw. Res.* 67, 163–172.  
781 <https://doi.org/10.1071/MF14219>

782 Crosswell, J.R., Anderson, I.C., Stanhope, J.W., Van Dam, B., Brush, M.J., Ensign, S.,  
783 Piehler, M.F., McKee, B., Bost, M., Paerl, H.W., 2017. Carbon budget of a shallow,  
784 lagoonal estuary: Transformations and source-sink dynamics along the river-estuary-  
785 ocean continuum. *Limnol. Oceanogr.* 62, S29–S45.  
786 <https://doi.org/10.1002/lno.10631>

787 Cyronak, T., Andersson, A.J., D’Angelo, S., Bresnahan, P., Davidson, C., Griffin, A.,  
788 Kindeberg, T., Pennise, J., Takeshita, Y., White, M., 2018. Short-term spatial and  
789 temporal carbonate chemistry variability in two contrasting seagrass meadows:  
790 Implications for pH buffering capacities. *Estuaries and Coasts* 41, 1282–1296.  
791 <https://doi.org/10.1007/s12237-017-0356-5>

792 Dickson, A.G., 1990. Standard potential of the reaction:  $\text{AgCl(s)} + 1/2\text{H}_2\text{(g)} = \text{Ag(s)} +$   
793  $\text{HCl(aq)}$ , and the standard acidity constant of the ion  $\text{HSO}_4^-$  in synthetic sea  
794 water from 273.15 to 318.15 K. J. Chem. Thermodyn. 22, 113–127.  
795 [https://doi.org/10.1016/0021-9614\(90\)90074-Z](https://doi.org/10.1016/0021-9614(90)90074-Z)

796 Ekstrom, J. a., Suatoni, L., Cooley, S.R., Pendleton, L.H., Waldbusser, G.G., Cinner, J.E.,  
797 Ritter, J., Langdon, C., van Hooidek, R., Gledhill, D., Wellman, K., Beck, M.W.,  
798 Brander, L.M., Rittschof, D., Doherty, C., Edwards, P.E.T., Portela, R., 2015.  
799 Vulnerability and adaptation of US shellfisheries to ocean acidification. Nat. Clim.  
800 Chang. 5, 207–214. <https://doi.org/10.1038/nclimate2508>

801 Gattuso, J., Epitalon, J., Lavigne, H. and Orr, J. (2021). seacarb: Seawater Carbonate  
802 Chemistry. R package version 3.2.15. <https://CRAN.R-project.org/package=seacarb>

803 Gazeau, F., Quiblier, C., Jansen, J.M., Gattuso, J.-P., Middelburg, J.J., Heip, C.H.R., 2007.  
804 Impact of elevated  $\text{CO}_2$  on shellfish calcification. Geophys. Res. Lett. 34, L07603.  
805 <https://doi.org/10.1029/2006GL028554>

806 Gobler, C.J., Talmage, S.C., 2014. Physiological response and resilience of early life-  
807 stage Eastern oysters (*Crassostrea virginica*) to past, present and future ocean  
808 acidification. Conserv. Physiol. 2, 1–15.  
809 <https://doi.org/10.1093/conphys/cou004>.Introduction

810 Ho, D.T., Law, C.S., Smith, M.J., Schlosser, P., Harvey, M., Hill, P., 2006.  
811 Measurements of air-sea gas exchange at high wind speeds in the Southern Ocean:  
812 Implications for global parameterizations. Geophys. Res. Lett. 33, 1–6.  
813 <https://doi.org/10.1029/2006GL026817>

814 Hofmann, G.E., Smith, J.E., Johnson, K.S., Send, U., Levin, L. a, Micheli, F., Paytan, A.,



815 Price, N.N., Peterson, B., Takeshita, Y., Matson, P.G., Crook, E.D., Kroeker, K.J.,  
816 Gambi, M.C., Rivest, E.B., Frieder, C. a, Yu, P.C., Martz, T.R., 2011. High-  
817 frequency dynamics of ocean pH: a multi-ecosystem comparison. PLoS One 6,  
818 e28983. <https://doi.org/10.1371/journal.pone.0028983>

819 Hsu S. A., 1994. Determining the power-law wind-profile exponent under near-neutral  
820 stability condidtions at sea. J. Appl. Meteorol. 33, 757–765.

821 Hu, X., Beseres Pollack, J., McCutcheon, M.R., Montagna, P. a., Ouyang, Z., 2015.  
822 Long-term alkalinity decrease and acidification of estuaries in Northwestern Gulf of  
823 Mexico. Environ. Sci. Technol. 49, 3401–3409. <https://doi.org/10.1021/es505945p>

824 Hu, X., Nuttall, M.F., Wang, H., Yao, H., Staryk, C.J., McCutcheon, M.R., Eckert, R.J.,  
825 Embesi, J.A., Johnston, M.A., Hickerson, E.L., Schmahl, G.P., Manzello, D.,  
826 Enochs, I.C., DiMarco, S., Barbero, L., 2018. Seasonal variability of carbonate  
827 chemistry and decadal changes in waters of a marine sanctuary in the Northwestern  
828 Gulf of Mexico. Mar. Chem. 205, 16–28.  
829 <https://doi.org/10.1016/j.marchem.2018.07.006>

830 Jiang, L.-Q., Cai, W.-J., Wang, Y., 2008. A comparative study of carbon dioxide  
831 degassing in river- and marine-dominated estuaries. Limnol. Oceanogr. 53, 2603–  
832 2615. <https://doi.org/10.4319/lo.2008.53.6.2603>

833 Jiang, L.Q., Cai, W.J., Wang, Y., Bauer, J.E., 2013. Influence of terrestrial inputs on  
834 continental shelf carbon dioxide. Biogeosciences 10, 839–849.  
835 <https://doi.org/10.5194/bg-10-839-2013>

836 Kealoha, A.K., Shamberger, K.E.F., DiMarco, S.F., Thyng, K.M., Hetland, R.D.,  
837 Manzello, D.P., Slowey, N.C., Enochs, I.C., 2020. Surface water CO<sub>2</sub> variability in

838 the Gulf of Mexico (1996–2017). *Sci. Rep.* 10, 1–13.  
839 <https://doi.org/10.1038/s41598-020-68924-0>

840 Laruelle, G.G., Cai, W.-J., Hu, X., Gruber, N., Mackenzie, F.T., Regnier, P., 2018.  
841 Continental shelves as a variable but increasing global sink for atmospheric carbon  
842 dioxide. *Nat. Commun.* 9, 454. <https://doi.org/10.1038/s41467-017-02738-z>

843 Li, D., Chen, J., Ni, X., Wang, K., Zeng, D., Wang, B., Jin, H., Huang, D., Cai, W.J.,  
844 2018. Effects of biological production and vertical mixing on sea surface pCO<sub>2</sub>  
845 variations in the Changjiang River Plume during early autumn: A buoy-based time  
846 series study. *J. Geophys. Res. Ocean.* 123, 6156–6173.  
847 <https://doi.org/10.1029/2017JC013740>

848 Mathis, J.T., Pickart, R.S., Byrne, R.H., Mcneil, C.L., Moore, G.W.K., Juranek, L.W.,  
849 Liu, X., Ma, J., Easley, R.A., Elliot, M.M., Cross, J.N., Reisdorph, S.C., Bahr, F.,  
850 Morison, J., Lichendorf, T., Feely, R.A., 2012. Storm-induced upwelling of high  
851 pCO<sub>2</sub> waters onto the continental shelf of the western Arctic Ocean and implications  
852 for carbonate mineral saturation states. *Geophys. Res. Lett.* 39, 4–9.  
853 <https://doi.org/10.1029/2012GL051574>

854 McCutcheon, M.R., Staryk, C.J., Hu, X., 2019. Characteristics of the carbonate system in  
855 a semiarid estuary that experiences summertime hypoxia. *Estur. Coast.* 42, 1509–  
856 1523. <https://doi.org/10.1007/s12237-019-00588-0>

857 Millero, F.J., 2010. Carbonate constant for estuarine waters. *Mar. Freshw. Res.* 61, 139–  
858 142.

859 Montagna, P.A., Brenner, J., Gibeaut, J., Morehead, S., 2011. Chapter 4: Coastal Impacts,  
860 in: Jurgen Schmandt, Gerald R. North, and J.C. (Ed.), *The Impact of Global*

861 Warming on Texas. University of Texas Press, pp. 96–123.

862 R Core Team (2020). R: A language and environment for statistical computing. R Founda  
863 tion for Statistical Computing, Vienna, Austria. URL <https://www.R-project.org/>.

864 Raymond, P.A., Cole, J.J., 2001. Gas exchange in rivers and estuaries: Choosing a gas  
865 transfer velocity. *Estuaries* 24, 312–317. <https://doi.org/10.2307/1352954>

866 Robbins, L.L., Lisle, J.T., 2018. Regional acidification trends in florida shellfish  
867 estuaries: a 20+ year look at pH, oxygen, temperature, and salinity. *Estur. Coast.* 41,  
868 1268–1281. <https://doi.org/10.1007/s12237-017-0353-8>

869 Sastri, A.R., Christian, J.R., Achterberg, E.P., Atamanchuk, D., Buck, J.J.H., Bresnahan,  
870 P., Duke, P.J., Evans, W., Gonski, S.F., Johnson, B., Juniper, S.K., Mihaly, S.,  
871 Miller, L.A., Morley, M., Murphy, D., Nakaoka, S.I., Ono, T., Parker, G., Simpson,  
872 K., Tsunoda, T., 2019. Perspectives on in situ sensors for ocean acidification  
873 research. *Front. Mar. Sci.* 6, 1–6. <https://doi.org/10.3389/fmars.2019.00653>

874 Schulz, K.G., Riebesell, U., 2013. Diurnal changes in seawater carbonate chemistry  
875 speciation at increasing atmospheric carbon dioxide. *Mar. Biol.* 160, 1889–1899.  
876 <https://doi.org/10.1007/s00227-012-1965-y>

877 Seim, H.E., Kjerfve, B., Sneed, J.E., 1987. Tides of Mississippi Sound and the adjacent  
878 continental shelf. *Estuar. Coast. Shelf Sci.* 25, 143–156.  
879 [https://doi.org/10.1016/0272-7714\(87\)90118-1](https://doi.org/10.1016/0272-7714(87)90118-1)

880 Semesi, I.S., Beer, S., Björk, M., 2009. Seagrass photosynthesis controls rates of  
881 calcification and photosynthesis of calcareous macroalgae in a tropical seagrass  
882 meadow. *Mar. Ecol. Prog. Ser.* 382, 41–47. <https://doi.org/10.3354/meps07973>

883 Solis, R.S., Powell, G.L., 1999. Hydrography, Mixing Characteristics, and Residence

884 Time of Gulf of Mexico Estuaries, in: Bianchi, T.S., Pennock, J.R., Twilley, R.R.  
885 (Eds.), Biogeochemistry of Gulf of Mexico Estuaries. John Wiley & Sons, Inc: New  
886 York, pp. 29–61.

887 Takahashi, T., Sutherland, S.C., Sweeney, C., Poisson, A., Metzl, N., Tilbrook, B., Bates,  
888 N., Wanninkhof, R., Feely, R.A., Sabine, C., Olafsson, J., Nojiri, Y., 2002. Global  
889 sea-air CO<sub>2</sub> flux based on climatological surface ocean pCO<sub>2</sub>, and seasonal  
890 biological and temperature effects. Deep. Res. Part II 49, 1601–1622.  
891 [https://doi.org/10.1016/S0967-0645\(02\)00003-6](https://doi.org/10.1016/S0967-0645(02)00003-6)

892 Thurman, H. V., 1994. Introductory Oceanography, Seventh Edition. pp. 252–276.

893 Uppström, L.R., 1974. The boron/chlorinity ratio of deep-sea water from the Pacific  
894 Ocean. Deep. Res. Oceanogr. Abstr. 21, 161–162. [https://doi.org/10.1016/0011-](https://doi.org/10.1016/0011-7471(74)90074-6)  
895 [7471\(74\)90074-6](https://doi.org/10.1016/0011-7471(74)90074-6)

896 USGS, 2001. Discharge Between San Antonio Bay and Aransas Bay, Southern Gulf  
897 Coast, Texas, May-September 1999.

898 Waldbusser, G.G., Salisbury, J.E., 2014. Ocean acidification in the coastal zone from an  
899 organism’s perspective: multiple system parameters, frequency domains, and  
900 habitats. Ann. Rev. Mar. Sci. 6, 221–47. [https://doi.org/10.1146/annurev-marine-](https://doi.org/10.1146/annurev-marine-121211-172238)  
901 [121211-172238](https://doi.org/10.1146/annurev-marine-121211-172238)

902 Wanninkhof, R., 1992. Relationship between wind speed and gas exchange. J. Geophys.  
903 Res. 97, 7373–7382. <https://doi.org/10.1029/92JC00188>

904 Wanninkhof, R., Asher, W.E., Ho, D.T., Sweeney, C., McGillis, W.R., 2009. Advances  
905 in quantifying air-sea gas exchange and environmental forcing. Ann. Rev. Mar. Sci.  
906 1, 213–244. <https://doi.org/10.1146/annurev.marine.010908.163742>

907 Weiss, R.F., 1974. Carbon dioxide in water and seawater: the solubility of a non-ideal  
908 gas. *Mar. Chem.* 2, 203–215.

909 Westfall, P.H., 1997. Multiple testing of general contrasts using logical constraints and  
910 correlations. *J. Am. Stat. Assoc.* 92, 299–306.  
911 <https://doi.org/10.1080/01621459.1997.10473627>

912 Yao, H., Hu, X., 2017. Responses of carbonate system and CO<sub>2</sub> flux to extended drought  
913 and intense flooding in a semiarid subtropical estuary. *Limnol. Oceanogr.* 62, S112–  
914 S130. <https://doi.org/10.1002/lno.10646>

915 Yao, H., McCutcheon, M.R., Staryk, C.J., Hu, X., 2020. Hydrologic controls on CO<sub>2</sub>  
916 chemistry and flux in subtropical lagoonal estuaries of the northwestern Gulf of  
917 Mexico. *Limnol. Oceanogr.* 1–19. <https://doi.org/10.1002/lno.11394>

918 Yates, K.K., Dufore, C., Smiley, N., Jackson, C., Halley, R.B., 2007. Diurnal variation of  
919 oxygen and carbonate system parameters in Tampa Bay and Florida Bay. *Mar.*  
920 *Chem.* 104, 110–124. <https://doi.org/10.1016/j.marchem.2006.12.008>

921